Tribology International 59 (2013) 154–162

Contents lists available at SciVerse ScienceDirect

Tribology International

journal homepage: www.elsevier.com/locate/triboint

Quantification of first contact detection errors on hardness and indentation size effect measurements

J. Marteau [a,*], M. Bigerelle [a,b], Y. Xia [a], P.-E. Mazeran [a], S. Bouvier [a]

[a] Laboratoire Roberval, UMR 6253, Université de Technologie de Compiègne, Centre de Recherches de Royallieu, BP 20529, 60205 Compiègne Cedex, France
[b] Laboratoire Thermique, Energétique, Mise en forme, Production, EA 4542, Université de Valenciennes et du Hainaut Cambrésis, Le Mont Houy, 59313 Valenciennes, France

ARTICLE INFO

Article history:
Received 31 August 2011
Received in revised form
25 June 2012
Accepted 27 June 2012
Available online 4 July 2012

Keywords:
Nanoindentation
Macrohardness
Contact
Size effect

ABSTRACT

A new method is proposed for the quantification of macroscopic hardness and indentation size effect. This method is based on the simultaneous treatment of several nanoindentation loading curves which are located according to the gap between their shape and the one predicted by the Bernhardt law. By applying this method on stainless steel loading curves, it is shown that hardness error can be reduced by a factor of 2 compared with usual treatment methods. It is shown that only the simultaneous treatment of all the curves enables the good prediction of pile-up in the material.

1. Introduction

Studying tribological behavior implies a characterization of the mechanical parameters of a material surface. Hardness tests and more recently instrumented indentation are specially adapted to study material surface properties. These tests are used to characterize polymers [1,2] as well as metals [3] or composite materials [4]. Hardness is a particularly interesting property as it plays an important role in the third-body wear [5] or in cavitation wear [6] and helps building analytical models (e.g. for scratch tests [7,8]).

Even though hardness tests are usually easy and convenient, they remain difficult to interpret. The first difficulty comes from the understanding of the complex stress field that is produced during indentation. This lack of understanding led to development of numerical simulations e.g. [9]. The second difficulty arises from metrological issues such as the detection of the first contact between the sample and the indenter [10–13]. An accurate determination of the indenter–sample first contact is crucial. It directly affects the measurement of the indentation depth and therefore the value of hardness or the results of models based on instrumented indentation curves [14]. Error in the first contact detection can also lead to a false identification of indentation size effects [15].

Several methods are developed to estimate the initial contact [16]. One of them is based on the detection of an initial contact force set by the user. The penetration depth corresponding to this force is set to zero. At the end of the test, the experimental data is fit using a smooth curve. The extrapolation of its y-intercept gives a measure of the initial penetration depth which is added to the recorded indentation depth. Another method sets the indentation depth to zero when the stiffness exceeded a value chosen by the user. In spite of these methods, the indenter–sample first contact remains uncertain and still affects the load versus indentation depth curves.

The present work is focused on the quantification of the errors affecting hardness and the identification of indentation size effects due to an incorrect detection of the first indenter–sample contact in nanoindentation. This quantification is made through the comparison of the results given by usual data treatment methods with our methodology which is based on two innovative concepts. The first one consists in marking off the curves thanks to the gap existing between their actual shape and a chosen behavior law to predict the instrumented indentation curve. The chosen behavior is Bernhardt's law [17] which takes into account the indentation size effects in the description of load versus indentation depth curve. This idea contrasts with the usual treatment methods which consider the zero-point as an absolute frame of reference. The second innovative concept of our method lies in the use of the curves for calculation of the set of mechanical parameters. Our method is based on the treatment of all the curves as a whole i.e. the mechanical properties are determined by minimizing a function that deals with all the curves.

* Corresponding author. Tel.: +33 3 44 23 73 34; fax: +33 3 44 23 49 84.
E-mail address: julie.marteau@utc.fr (J. Marteau).

0301-679X/$ - see front matter © 2012 Elsevier Ltd. All rights reserved.
http://dx.doi.org/10.1016/j.triboint.2012.06.029

This concept differs from usual data treatment methods as they use only one curve to calculate a set of mechanical parameters. Then the results given by different curves are gathered and averaged.

The robustness of our method compared with usual treatments is evaluated using the instrumented indentation curves of 100 nanoindentation tests. The indents are made on 316L stainless steel specimens having rough to mirror-like surfaces respectively corresponding to the use of polishing papers from 80 to 4000 grit. Using different magnitudes of deterioration of the surface will help evaluating the robustness of the methods. Several intermediate data treatment methods will also be tested to show the relevance of our hypotheses and the improvements given by our methodology.

The paper is divided into five main parts. The second section is devoted to the description of the material and the experimentations. The third part is focused on the description of the law behavior considered in this study and the data treatment methods which ensue. The fourth section is dedicated to the comparison of the results given by our method with several other data treatment methods. Their advantages, drawbacks and robustness are evaluated. Finally, the Conclusion will summarize the main findings of the paper.

2. Material and methods

2.1. Material

The material used in this study is 316L stainless steel. The samples are cut from a 30 mm rod into 20 mm thick disks. This material is composed of a single austenitic phase. However, mechanical polishing can induce a martensitic transformation due to local stresses between the abrasive grains and the surface [18]. Strain-hardening can thus be reinforced by this transformation. The chemical composition of this steel is given in Table 1.

2.2. Mechanical polishing

The 316L specimens are polished using an automatic grinding machine having off-centered rotating movements. First, all the specimens are polished to a mirror-like surface i.e. to silicon carbide paper grit 4000 to obtain similar initial states. The surface history of the specimen is also guaranteed by the use of a new grit paper at each polishing step.

Then, several magnitudes of damage are achieved by using different grit papers under identical force and time conditions (150 N, 3 min) with water lubrication. The different surface states correspond to the ending of the abrasion after using grit papers: 80, 120, 180, 220, 320, 500, 800, 1000, 1200, 2400 or 4000. In the following, 11 specimens will be denoted using the number of the final paper used to polish them.

2.3. Roughness measurements

The topography of the abraded samples is measured using a three dimensional roughness tactile profilometer: TENCOR™ P10. Roughness is recorded with a 2 μm tip stylus under a load of 5×10^{-5} N with a vertical resolution of the nanometer order. In order to evaluate the topography texture, a series of tridimensional preliminary measurements is practiced on 4×4 mm^2 areas. These results show that a hypothesis of isotropy can be supported. The specimen topography is then analyzed more accurately using two dimensional profiles recorded on a 5 mm length with a higher sampling frequency. For each specimen, 30 two dimensional profiles of 25,000 points are recorded randomly on the surface with a 200 μm/s speed.

2.4. Nanoindentation tests

Nanoindentation tests are made with a Nano Indenter XP®, equipped with a Berkovich indenter at ambient temperature. Using the Continuous Measurement Method (CSM) with a constant strain rate equal to 0.05 s^{-1}, a maximum indentation depth of 3 μm is achieved. One hundred indentations are made into each 316L specimen. Fig. 1 shows the load versus indentation depth curves obtained for a specimen polished with paper grit 4000. Only the loading parts of the curves are shown.

The one hundred curves obtained for the eleven samples are then prepared for the data treatment methods. This preparation is composed of three pretreatments. The first one isolates the loading part of the instrumented indentation curve as it will be the only part considered in this study. The second pretreatment consists in re-sampling the experimental indentation depth to obtain independence and identical distribution values in order to avoid statistical artifacts. Finally, using the Oliver and Pharr method [19], the contact depth h_c is extracted from nanoindentation data applying the following formula:

$$h_c = h - \varepsilon P/S, \tag{1}$$

where h_c is the contact depth, S is the stiffness and ε is a geometrical constant equal to 0.75 for a Berkovich indenter.

A complete description of these pretreatments can be found in [20].

3. Theory and data treatment methods

3.1. Behavior laws

For geometrically similar indenters, the loading part of the instrumented indentation curves is usually described using a

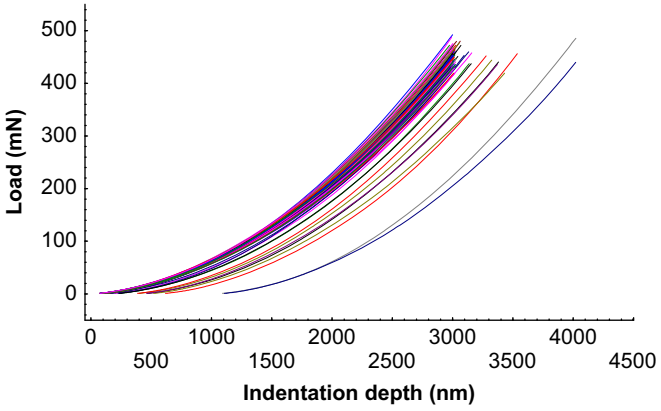

Fig. 1. Load (mN) versus indentation depth (nm) curves for 316L stainless steel specimens polished with paper grit 4000.

Table 1
Chemical composition of the 316L stainless steel rod.

Chemical elements	C	Si	Mn	Ni	Cr	Mo	N	S	P	Cu	Fe
Weight percent	0.008	0.27	1.62	14.58	17.58	2.8	0.060	0.001	0.014	0.070	Bal.

parabolic relationship between the load P and the indentation depth h. This model is known as Kick's law [21] and is expressed as follows:

$$P = Ch^2, \tag{2}$$

where C is a constant depending on the geometry of the indenter tip and the material properties.

However, this simple model has rapidly become insufficient to describe the experimental curves. Zeng and Chiu [22] have shown that this model cannot describe the beginning of the loading curve for several materials, including aluminum or fused silica.

Earlier, Bernhardt [17] also noticed this deviation and proposed correcting Kick's formula by adding a linear term:

$$P = \left\{\alpha_1 h^2 + \alpha_2 h\right\}, \tag{3}$$

where α_1 and α_2 are constants depending on the geometry of the indenter tip and the material properties. The inclusion of the linear term is used to characterize the load dependence with increasing indentation depth at the beginning of the P–h curve.

Bernhardt's law can be expressed with the contact area h_c defined in Eq. (1) and rewritten as follows:

$$P = \alpha\left\{H_0 h_c^2 + \beta h_c\right\}, \tag{4}$$

where α is a constant depending on the geometry of the indenter, H_0 is the macrohardness of the specimen and β is the indentation size effect (ISE) factor.

From this equation, we assume that the experimental curves can show a deviation Δh_c from this model according to the indentation depth axis. This deviation can be induced by a wrong detection of the first contact or the presence of roughness. The addition of a deviation Δh_c to the contact depth h_c in Eq. (4) gives the following formula:

$$P = \alpha\left\{H_0(h_c + \Delta h_c)^2 + \beta(h_c + \Delta h_c)\right\} \tag{5}$$

Once Eq. (5) is developed and reorganized, the following equation is obtained:

$$P = \alpha\left\{H_0 h_c^2 + (2H_0\,\Delta h_c + \beta)h_c + H_0\,\Delta h_c^2 + \beta\,\Delta h_c\right\}. \tag{6}$$

Eq. (6) is the basis for the development of data treatment methods.

3.2. Data treatment methods

This section introduces the equations allowing the treatment of instrumented indentation data to determine the macrohardness and the ISE factor of the studied material. The first part shows the formula describing the treatment of the curves as separate entities. The second part describes the philosophy of our methodology which treats the one hundred curves as a whole to calculate the mechanical properties. In the last part, intermediary versions of the previous methods are introduced in order to assess the validity of the considered hypotheses.

3.2.1. Individual treatment of the curves

The individual treatment of the load versus depth curves presented here is related to the methods usually used to analyze indentation data. This treatment implies the calculation of one set of mechanical parameters with the use of only one curve. It means that one hundred curves give one hundred sets of parameters. These sets are then averaged to obtain a single value for each mechanical parameter.

A first step to identify the macrohardness and the ISE factor included in Eq. (6) consists in minimizing the following function:

$$\min_{H_{0,i},\Delta h_i,\beta_i} \sum_{j=1}^{p_i} \left[P_{i,j} - \alpha\left(H_{0,i} h_{c,j}^2 + (2H_{0,i}\,\Delta h_{c,i} + \beta_i)h_{c\ j} + H_0\,\Delta h_{c,i}^2 + \beta_i\,\Delta h_{c,i}\right)\right]^2, \tag{7}$$

where j refers to a point in curve number i and Δh_{ci} is the deviation of curve i from Bernhardt's law.

Once this minimization is achieved for all the curves, the average of the macrohardness and the ISE factor is calculated as follows:

$$\overline{H_0} = \frac{1}{n}\sum_{i=1}^{n}\left[H_{0,i}\right], \tag{8}$$

$$\overline{\beta} = \frac{1}{n}\sum_{i=1}^{n}\left[\beta_i\right]. \tag{9}$$

The use of only one curve for the calculation of two factors may affect the robustness of the method. This hypothesis led us to develop a new method which deals with all the curves as a whole.

3.2.2. Simultaneous treatment of the loading curves

To treat all the loading curves simultaneously, the following hypothesis is made: the macrohardness and the ISE factor are homogeneous for all the studied specimens. Thus, treating all the curves as a whole gives only one set of mechanical parameters. From this hypothesis and Eq. (6), the following function is built for minimization:

$$\min_{H_0,\Delta h_1,\ldots,\Delta h_n,\beta} \sum_{i=1}^{n}\sum_{j=1}^{p_i} \left[P_{i,j} - \alpha\left(H_0\, h_{c,j}^2 + (2H_0\,\Delta h_{c,i} + \beta)h_{c\ j} + H_0\,\Delta h_{c,i}^2 + \beta\,\Delta h_{c,i}\right)\right]^2, \tag{10}$$

where j refers to a point belonging to curve i.

3.2.3. Intermediary treatments

In order to check the validity of the hypotheses of the chosen model, intermediary pretreatments are built. These pretreatments are qualified as "intermediary" because they come from several variations of the previous treatment methods.

The first variation concerns the referential choice. Our treatment methods suppose that all the curves are linked by a gap, Δh_c, between their actual shape and the shape predicted by Bernhardt's law. To show the validity of the chosen referential, it is compared with two other definitions of the first contact. One definition assumes that the zero set by the device is the actual one. Thus, the gap $\Delta h_{c,i}$ is equal to zero in Eqs. (7) and (10). In the other referential, the first contact point is defined for a load equal to zero. This definition of the zero is applied by shifting all the loading curves according to the indentation depth axis. Then, all the loading curves are treated considering Eqs. (7) and (10) with $\Delta h_{c,i}$ equal to zero.

The last variation deals with the indentation size effect. We have chosen to take it into account during the pretreatment of the curves but, usually this effect is ignored. Ignoring this effect implies that the loading curves are treated using Kick's law. In our case, it means that the ISE factor, β_i (respectively β) is equal to zero in Eq. (7) (respectively 10).

In the following section, our method is called Method A and is compared with five other methods (Method B,–F) built with the previous considerations.

4. Results and discussion

To properly compare the results given by the different treatment models, confidence intervals on H_0 and β are needed. The confidence intervals are determined using a double Bootstrap on the 100 experimental loading curves of each specimen. The first Bootstrap is used to simulate noise in a given loading curve. The second Bootstrap permits practicing a simple random sampling with replacement. This sampling method is repeated 1000 times to reproduce the specimen heterogeneity.

This section is divided into three main parts. First, the influence of the referential choice on the macrohardness and the ISE factor is investigated. Then, the advantage of treating all the loading curves as a whole instead of calculating several mechanical parameters on only one curve is analyzed. Finally, our model is validated by comparing its results with other intermediary methods ignoring the indentation size effect.

4.1. Referential choice influence

The need for a better knowledge of material surface properties at nanoscales implies the reduction of measurement errors and uncertainties. An important source of error in nanoindentation tests is caused by the first contact position identification. In spite of the accuracy improvement of measurement devices, its position remains uncertain. Its bad identification can seriously deteriorate mechanical characteristics such as hardness. To minimize the errors caused by the first contact identification, several methods were developed. Usual methods define the first contact with the help of a particular point or value. They use an absolute referential. On the contrary, our method is based on the use of a relative referential. The position of the curves is defined using the gap existing between the shape of the loading curves and the shape predicted by the Bernhardt model [17] as defined in Eq. (10). In this section, the results given by our treatment method, called Method A, are compared with a second method, called Method B, which assumes that the first contact occurs when the load is equal to zero. Thus, all the experimental loading curves are shifted according to the x-axis before the minimization described by the following equation:

$$\min_{H_0,\beta} \sum_{i=1}^{n} \sum_{j=1}^{p_i} \left[P_{i,j} - \alpha\left(H_0 h_{c,j}^2 + \beta h_{c\ j}\right)\right]^2. \quad (11)$$

For more clarity, Table 2 summarizes different methods and hypotheses studied in this paper.

Figs. 2 and 3 show the shifting of the curves using our Method A and Method B for Specimen 4000, respectively. Compared with Fig. 1 displaying the experimental loading curves, there is an important decrease of the scatter using both methods.

Table 2
Summary of the method hypotheses. The individual methods treat each curve separately while the simultaneous method treats all the curves as a whole. The ISE consideration means that Bernhardt's law is used for the treatment; otherwise Kick's law is used. The shifting of the curves is either done considering the gaps between the loading curve shapes and Bernhardt's law prediction or by assuming that the first contact occurs when the load is equal to zero.

Method	Individual/simultaneous treatment	ISE consideration ($\beta \neq 0$)	Shifting of the curves
A	Simultaneous	Yes	Use of Δh_c
B	Simultaneous	Yes	Use of $P=0$
C	Individual	Yes	Use of Δh_c
D	Simultaneous	No	No shift
E	Simultaneous	No	Use of Δh_c
F	Simultaneous	Yes	No shift

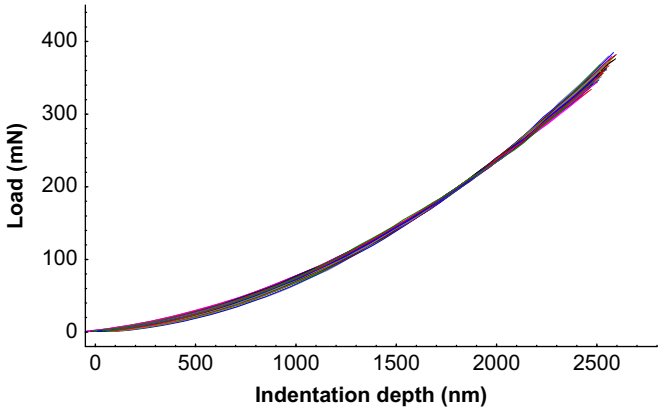

Fig. 2. Shifting of the loading curves of Specimen 4000 using the gaps existing between the loading curve shapes and the shape predicted by Bernhard's law (Method A).

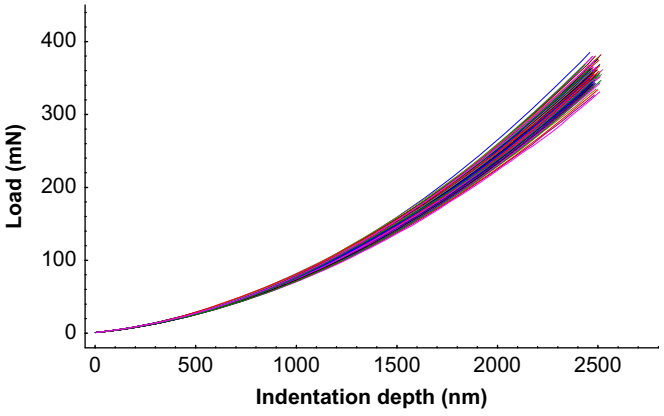

Fig. 3. Shifting of the loading curves of Specimen 4000 assuming the first contact occurs when the load is equal to zero (Method B).

Table 3
Macrohardness (H_0) and ISE factor (β) average and standard deviations obtained for Specimen 4000 using two treatment methods. The first treatment method, called Method A, considers a gap between Bernhardt's law prediction and the real shape of the loading curves. The second one, Method B, assumes the first contact occurs when the load is equal to zero.

Method	H_0 (GPa)		β (mN/nm)	
	Average	Standard deviation	Average	Standard deviation
A	1.863	0.004	1114	30
B	1.836	0.011	1271	29

With Method A, the curves are difficult to distinguish. On the contrary, Method B gives a more important scatter. This first comparison underlines the interest in considering the loading curves in relation to a given behavior instead of an arbitrary chosen value.

Thanks to the use of double Bootstrap for both treatment methods, the average values and the standard deviations are calculated for the macrohardness and the ISE factor. Table 3 summarizes the results obtained for Specimen 4000. The macrohardness average values are very close. Method B gives a macrohardness similar to that of our method. On the other hand, Method B has a standard deviation which is 2.5 times higher than the one given by our method (Method A). Thus, it shows that considering the curves with respect to a chosen behavior law gives a better accuracy for the determination of material

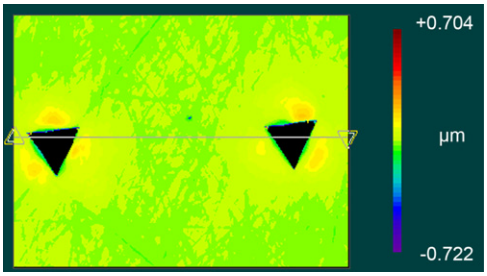

Fig. 4. Observation of piling-up occurring in 316L steel polished with paper grit 4000 using interferometric microscopy.

parameters than methods based on the consideration of arbitrary values.

The average values found for the ISE factor are also very close. The standard deviations are also nearly identical. The one calculated with Method B is only slightly smaller than the standard deviation of our method.

To check the validity of the results for the ISE factor value, the indentation prints made on Specimen 4000 are observed with interferometric microscopy. All the prints show piling-up. An example is given in Fig. 4. Piling-up observation indicates that positive values should be identified for the ISE factor [23]. As a consequence, both methods correctly describe the material behavior.

4.2. *Individual treatment versus simultaneous treatment*

It is worth noting that in our method, all the experimental loading curves are simultaneously handled. This choice stands against usual analyses which calculate one set of mechanical parameters per loading curve. The mechanical parameters are then averaged to obtain a better representativeness. However, the use of a single curve for the identification of several parameters can deteriorate its robustness and lead to errors. This second section is dedicated to the comparison of the robustness and errors made when using our treatment method (Method A) and the ones made when the curves are considered independently, hereafter referred to as Method C. The minimization corresponding to Method C is given by Eq. (7).

Both treatment methods are based on the optimization of a given function using a gradient descent. A mathematical optimization consists in minimizing the considered function by systematically choosing values in a defined domain. Due to the high nonlinearity of Eq. (10), an iterative scheme of optimization has to be used [24,25]. The Levenberg–Marquardt Algorithm is a very popular curve-fitting algorithm used in many software applications for solving generic curve-fitting problems. However, the Levenberg–Marquardt Algorithm finds only a local minimum, not a global minimum. Thus, as the function variations remain unknown, several starting points have to be tested to avoid mistaking a local minimum for a global one. When using different starting points, our method gives similar results (well posed problem). On the contrary, the method treating the curves separately leads to different results (ill-posed problem).

The shifting of the curves given by this method using three different starting points is displayed in Figs. 5–7. The curves in Fig. 5 clearly show a greater scatter than the shifting of our model depicted in Fig. 2. This tendency is even more pronounced when using the third starting point. The shifting given by the second starting point (Fig. 6) gives rise to two subpopulations. These first observations reveal that the method treating the curves separately is dependent on the initial values and thus unstable compared to our model. It is an ill-posed problem.

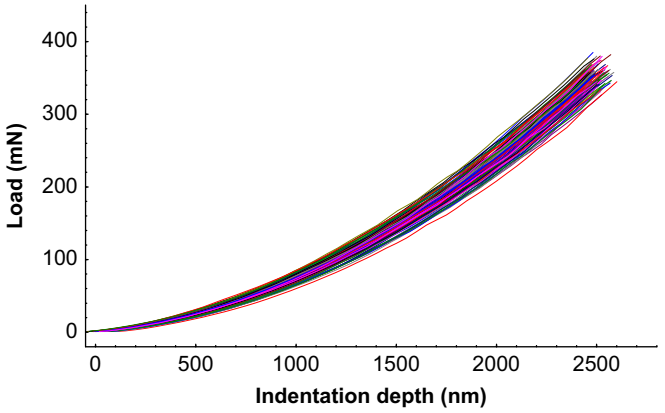

Fig. 5. Shifting of the loading curves obtained with the individual treatment method (Method C) using Starting point 1.

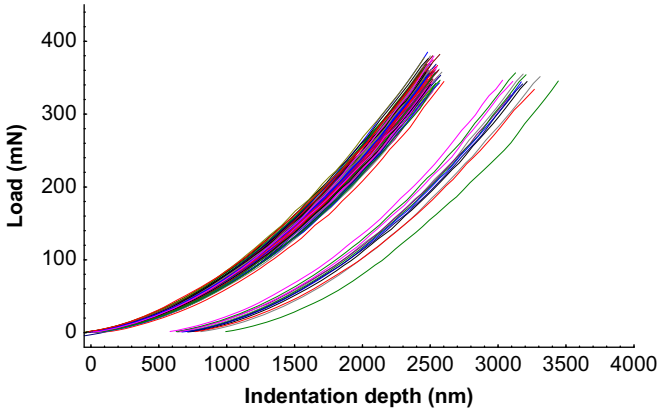

Fig. 6. Shifting of the loading curves obtained with the individual treatment method (Method C) using Starting point 2.

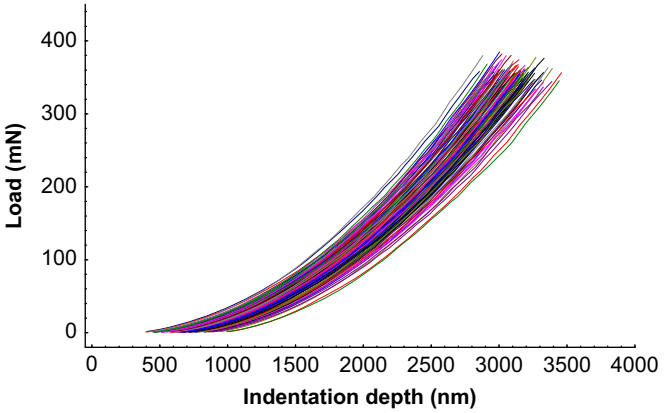

Fig. 7. Shifting of the loading curves obtained with the individual treatment method (Method C) using Starting point 3.

Table 4 further details the results given by the three starting points and indicates again the average and standard deviation values found with our model for the macrohardness and ISE factor. Whatever the method or the tested starting point, the average values obtained for the macrohardness are nearly identical. For the method treating all the curves separately, the macrohardness average is equal to 1.852 GPa while the standard deviation is spread out between 0.007 and 0.008 GPa. These values remain, certainly, low but only because hardness is determined using one hundred experimental curves. Moreover, the standard deviations calculated for Method A are approximately twice lower than the

Table 4
Average and standard deviation values obtained for the macrohardness (H_0) and the ISE factor (β) using the simultaneous treatment (Method A) and the individual treatment method (Method C) with 3 different starting points.

Method	H_0 (GPa)		β (mN/nm)	
	Average	Standard deviation	Average	Standard deviation
A	1.863	0.004	1114	30
C	1.852	0.007	1153	25
Starting point 1				
C	1.852	0.008	914	63
Starting point 2				
C	1.852	0.008	−1157	26
Starting point 3				

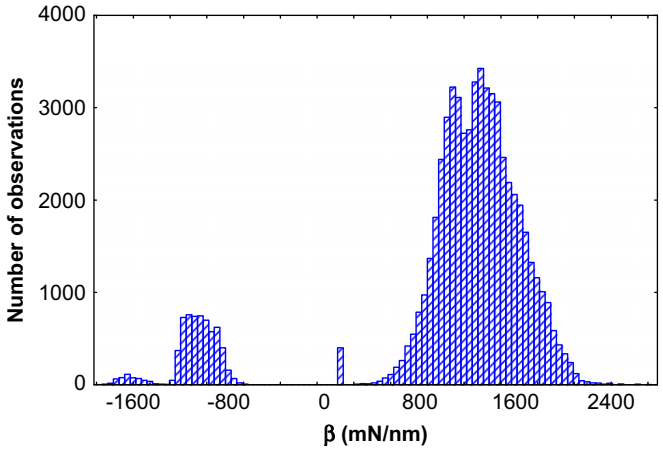

Fig. 8. ISE factor distribution using the individual treatment of the loading curves with the second starting point.

one given by Method C. If a Gaussian hypothesis is acceptable, it means that four times less experimental loading curves are needed with our method (Method A) to give the same results as those of Method C.

The ISE factor average values found for the three starting points are very different. The first starting point gives an average value equal to 1153 mN/nm which is similar to the one given by our method. Its standard deviation is on the same order of magnitude as the one corresponding to our model. On the other hand, the second starting point gives an average value which is 1.3 smaller than the ISE factor given by the first starting point while its standard deviation is 2.5 higher. Fig. 8 shows the distribution of the ISE factor values found for each curve using the second starting point. Two subpopulations of ISE factor can be distinguished. The first one shows a negative ISE factor while the second one has a positive ISE factor. These results explain why two subpopulations can be distinguished in Fig. 5 too. But the SEM observations show that only piling-up occurs in the material. It highlights the lack of robustness of the model treating the curves separately. This fact is confirmed by the ISE factor average given by the third starting point: a negative value is found with a standard deviation on the same order of magnitude as the one given by our model.

The standard deviations found using the first and the third points tend to be slightly smaller than the one given by our model. This tendency can be explained by a better fit of the curves with Model C. Indeed, each curve is fitted using a different value for the macrohardness and the ISE factor. Conversely, in our model, such values are supposed to be homogeneous.

It is important to note that the best results for the ISE factor and the macrohardness determination are found when the shifting of the curve is successful. To explain this tendency, the values of the gaps between the curve and the shape predicted by Bernhardt's model are studied as a function of the ISE factor value. Thousand couples of values are obtained using a Bootstrap enabling a random sampling with replacement. Fig. 9 shows the results given by Method C, treating the curves separately, using the first starting point. Fig. 10 illustrates the results given by our method treating all the curves as a whole.

In Fig. 9, the gaps between the curves decrease as the ISE factor increases from 0 to 2500 mN/nm for gaps ranging from −1200 to 200. This relationship clearly indicates that in Eq. (7), the ISE factor value depends on the value of the gap between the curve and the chosen model. These results explain why different results are obtained when using distinct starting points.

On the other hand, the gap values and the ISE factor seem to be independent for our model in Fig. 10. Indeed, the ISE factor varies only from 1010 to 1220 mN/nm for gaps ranging from −1100 to 20. It proves that the ISE factor value does not depend on the gap value. This last observation confirms that treating all the loading curves as a whole endows the method with robustness.

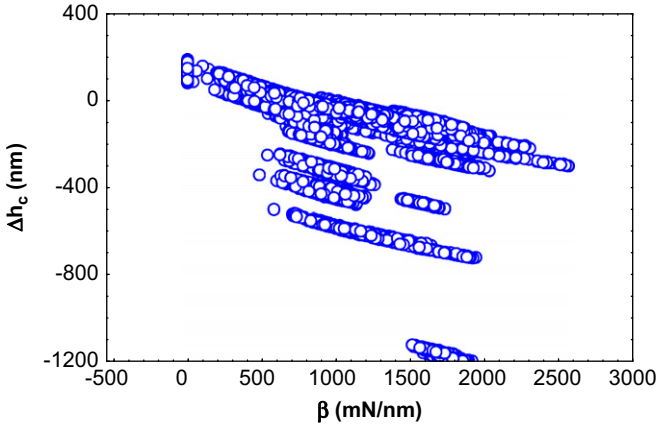

Fig. 9. Values of the gaps between the experimental loading curves and the shape predicted by Bernhardt's law (Method A) versus the ISE factor values for the individual treatment method (Method C) using the first starting point. One thousand couples of values are obtained using a Bootstrap.

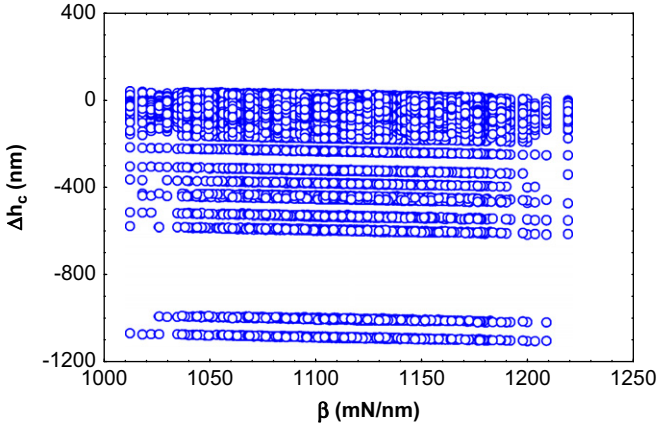

Fig. 10. Values of the gaps between the experimental loading curves and the shape predicted by Bernhardt's law versus the ISE factor values for the simultaneous treatment method (Method A). One thousand couples of values are obtained using a Bootstrap.

4.3. Application of the treatment method on rough surfaces

The improvements brought by our method have mainly been quantified by a statistical study. Now, its robustness is analyzed through its application to the experimental results of the eleven abraded specimens.

4.3.1. Real hardness and ISE

Our method (Method A) and intermediary methods, presented in Table 2, are applied to the loading curves of the specimens having different magnitudes of deterioration. All the considered methods treat the curves simultaneously but considering different hypotheses.

A first intermediary method, called Method D, ignores the indentation Size effect in its formulation; thus Kick's law is used for the behavior law. It also considers that the measurement device succeeds in the detection of the first indenter–sample contact. Thus, no zero detection correction is realized. This method is based on the following minimization:

$$\min_{H_0} \sum_{i=1}^{n} \sum_{j=1}^{p_i} \left[P_{i,j} - \alpha \left(H_0 h_{c,j}^2 \right) \right]^2 \tag{12}$$

The second intermediary method, called Method E, also ignores the ISE but takes into account the gaps between the loading curves and Bernhardt's model prediction. The third intermediary method, Method F, considers the ISE but no shifting of the curves is practiced.

The variation of the macrohardness calculated with the last four methods is depicted in Fig. 11 versus the specimen grit paper number. A dotted line stands for the experimental macrohardness measured on Specimen 4000.

Method F gives absurd values: a negative macrohardness is found for Specimen 80 and equal to zero for Specimens 220 and 1000. The other macrohardness values are also underestimated as a value equal to 1.00 GPa is obtained for Specimen 4000 while the experimental measurements gives 1.83 GPa. On the other hand, Method D tends to globally overestimate the macrohardness, except for Specimen 80, whose value is abnormally low as it is equal to 1.20 GPa.

Methods E and A show a variation of the macrohardness which meets expectations. Indeed, polishing with low grit papers (i.e. high abrasive size) tends to harden the surface of the material while these effects are less important with high paper grit (i.e. low abrasive size). Surface hardening can be also reinforced by the transformation of austenite into martensite due to friction [18]. Martensite being a harder component than austenite, an increase of the hardness is induced.

The macrohardness values are globally higher when calculated using Method E instead of Method A. For Specimen 80, Method E gives a macrohardness equal to 2.80 GPa while 2.20 GPa is obtained with Method A. The macrohardness values found for Specimen 4000 are closer as Method E gives 1.94 GPa and Method A gives 1.89 GPa. The global tendency to overestimate the macrohardness highlights the importance of considering indentation size effects (i.e. a linear relationship between the load and the indentation depth at the early stage of indentation) when analyzing the loading curves.

It should also be noted that Method A gives a slightly lower macrohardness for Specimen 80 than for Specimen 120. This evolution goes against our expectations. To try to explain this phenomenon, observations are made using Scanning Electron Microscopy. Fig. 12 shows the nanoindentation prints made on Specimen 80. It can be noticed that the nanoindentation print is less important than the one given by Specimen 4000 (Fig. 4). Due to the important high cross groove depth, it seems that the specimen tends to behave as a porous material which leads to a smaller macrohardness.

The ISE factor evolution as a function of the specimen numbers is depicted in Fig. 13. It can be noticed that Method A gives an ISE factor that decreases from about 4000 mN/nm to 1500 mN/nm with an increase of the paper grit number. Method F gives

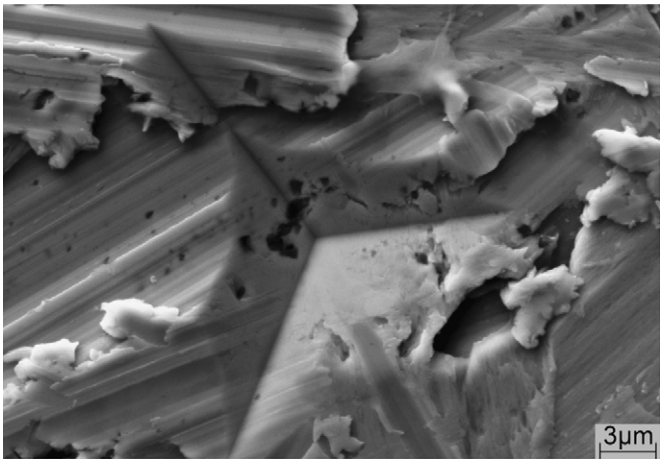

Fig. 12. Observation of the nanoindentation prints made in 316L steel polished with paper grit 80 using Scanning Electron Microscopy.

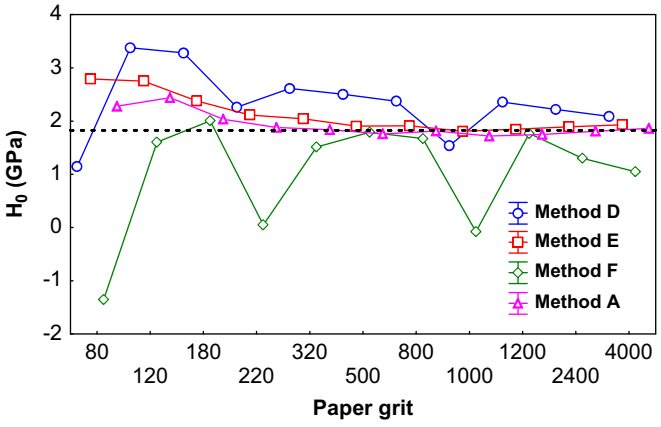

Fig. 11. Macrohardness values calculated for each abraded specimen using four treatment methods. Method hypotheses are summarized in Table 2. The dotted line stands for the macroscopic hardness measured with Specimen 4000.

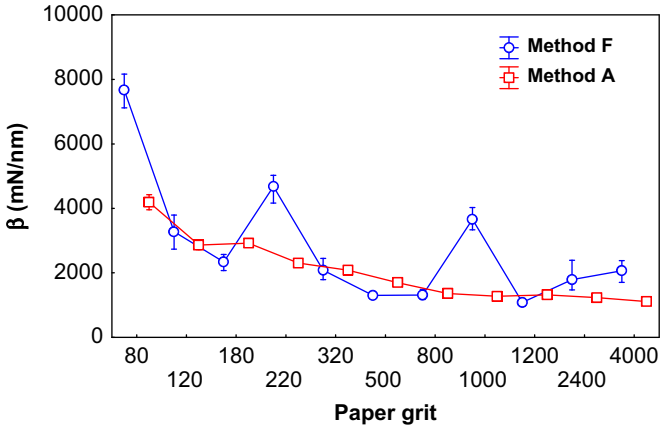

Fig. 13. ISE factor values calculated for each abraded specimen using two treatment methods. Method hypotheses are summarized in Table 2.

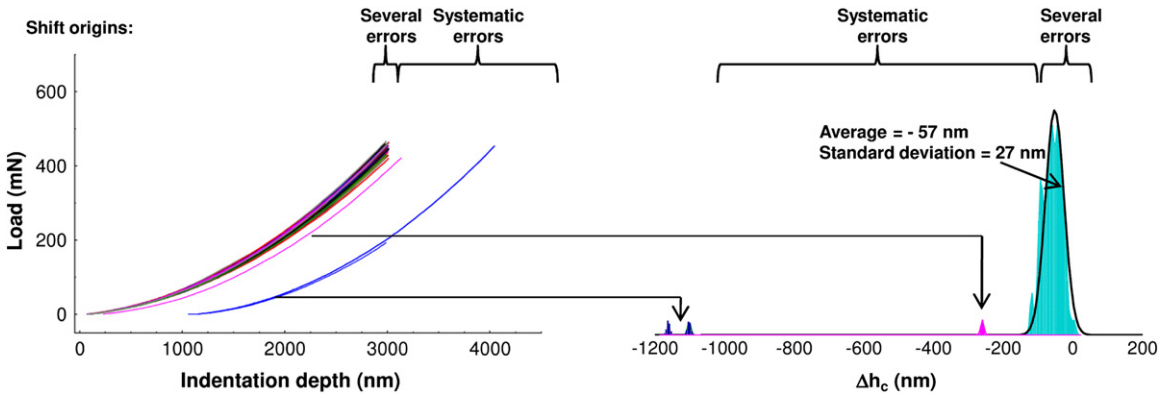

Fig. 14. Illustration of the origins of the gaps between the loading curve shapes and Bernhardt's prediction (Δh_c) using Specimen 2400 experimental loading curves and results for the gap distribution using a double Bootstrap.

fluctuating values with particularly high ISE factor for Specimens 80, 200 and 1000.

We previously observed that a decrease in the paper grit number gives higher macrohardness. This phenomenon is caused by surface hardening and the creation of stress-induced martensite [18]. According to [26,27], pile-up is greatest in materials that possess little capacity for strain-hardening. Martensite being harder than austenite [28], the formation of pile-up should be more important in specimens polished with low paper grit numbers. According to [23], a higher pile-up gives a greater ISE factor value. This observation corroborates the results given by our method as an increasing ISE factor is found for decreasing paper grit numbers (Fig. 13).

However, it is worth noting that the indentation size effect has different origins. For crystalline materials, it can be caused by specimen preparation problems (formation of hardened surface layers due to polishing or hard surface oxides), indenter tip blunting, roughness effects or false estimation of the surface contact (occurrence of pile-up). Microscopic phenomena can also be the origin of this effect. The apparition of geometrically necessary dislocations to accommodate the volume of material displaced by the indenter at the surface gives rise to an extra hardening [29,30].

To further assess our method robustness, the origin of the observed gaps between the curve shapes and Bernhardt's prediction are investigated.

4.3.2. Gap origin

The observation of the experimental load *versus* indentation depth curves enables the identification of two types of errors, whatever the paper used to polish the specimens, as illustrated in Fig. 14.

The first subpopulation gathers many curves showing a low scatter. Other curves show a low load for an important indentation depth: they are part of the second subpopulation. Both subpopulations are also noticeable when studying the distribution of the values of the gap between the loading curve shape and Bernhardt's prediction, as shown in Fig. 14.

The recording of important indentation depth for low loads is due to a false detection of the first contact by the nanoindentation device. It can be caused by surface contamination. It is a part of systematic errors. The first subpopulation arises from different phenomena such as measurement noise, indenter tip defect, temperature variation or roughness. Using the eleven abraded specimen topography results, the effect of roughness on Δh_c value is studied. For each sample, using the one hundred loading curves and a double Bootstrap, the standard deviation of Δh_c is computed. The calculated values are then presented in function of the Root-Mean-Square (RMS) roughness calculated using the topography results of each abraded specimen, as shown in Fig. 15.

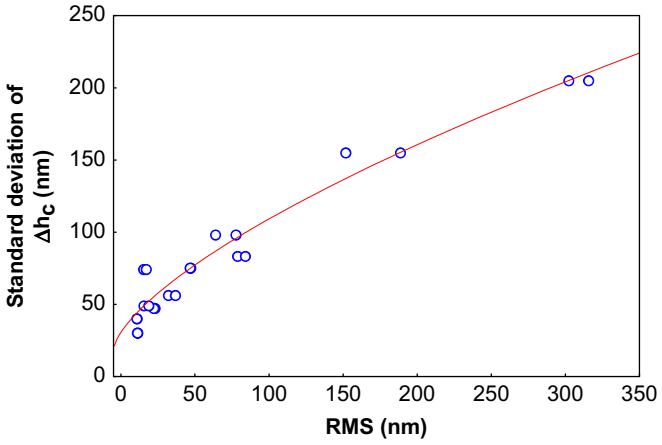

Fig. 15. Standard deviation of the gaps between the loading curve shapes and Bernhardt's prediction versus Root-Mean-Square (RMS) roughness.

The standard deviation of Δh_c and the Root-Mean-Square roughness increase from about 25 nm to 210 nm and from about 10 nm to 310 nm, respectively. Thus, a same order of magnitude is observed whatever the studied abraded specimen. It shows that the gaps between the loading curve shape and Bernhardt's prediction are caused by roughness. This final study corroborates the robustness of the proposed method.

By comparing the hypotheses of our method with usual considerations, we also emphasize the important scatter of the indentation data and its influence on the identification of the mechanical parameters. This identification is still discussed as illustrated by the various articles published on the subject (e.g. [31–33]). Therefore, in order to improve the accuracy in the identification of the mechanical parameters using nanoindentation, the analyses of the correlation that may exist between the defined parameters as well as the assessment of the impact of the position of the first contact point are highly required.

5. Conclusion

In this paper, an original treatment method of the nanoindentation loading curves is proposed for the determination of the macrohardness and the quantification of indentation size effects. The method is applied simultaneously to one hundred indentation

loading curves of a stainless steel considering a relative referential instead of an absolute referential used in standard treatment methods. This relative referential is based on the comparison of the gap existing between the shape predicted by Bernhardt′s law and the actual shape of the experimental loading curves. The main finding of the proposed work can be summarized as follows:

(i) The indentation size effect must be taken into account when treating the loading curves to determine the material hardness. Ignoring this effect leads to an overestimation of the material macrohardness. This effect is even more pronounced for non-mirror-like surfaces,
(ii) Considering the loading curves according to a gap between their real shape and Bernhardt′s law reduces the hardness error by a factor of 2.5,
(iii) More precise determination of the material macrohardness and indentation size effects requires a simultaneous use of several loading curves. The hardness error is reduced by a factor of 2 comparing with an individual treatment of the curves. Besides, quantifying the indentation size effect using only one curve can lead to misidentify the indentation size effect. Whatever the method used to identify material properties, it is crucial to evaluate the correlation between the defined parameters.

This original treatment method will be further assessed on other metallic materials such as Titanium based alloys.

References

[1] Briscoe BJ, Evans PD, Biswas SK, Sinha SK. The hardnesses of poly(methylmethacrylate). Tribology International 1996;29:93–104.
[2] Bhuyan S, Sundararajan S, Andjelkovic D, Larock R. Micro- and nanotribological behavior of soybean oil-based polymers of different crosslinking densities. Tribology International 2010;43:2231–9.
[3] Pelletier H. Predictive model to estimate the stress–strain curves of bulk metals using nanoindentation. Tribology International 2006;39:593–606.
[4] Sinha SK, Reddy SU, Gupta M. Scratch hardness and mechanical property correlation for Mg/SiC and Mg/SiC/Ti metal–matrix composites. Tribology International 2006;39:184–9.
[5] Axén N, Jacobson S, Hogmark S. Influence of hardness of the counterbody in three-body abrasive wear—an overlooked hardness effect. Tribology International 1994;27:233–41.
[6] Godoy C, Mancosu RD, Machado RR, Modenesi PJ, Avelar-Batista JC. Which hardness (nano or macrohardness) should be evaluated in cavitation? Tribology International 2009;42:1021–8.
[7] Williams JA. Analytical models of scratch hardness. Tribology International 1996;29:675–94.
[8] Briscoe BJ, Biswas SK, Sinha SK, Panesar SS. The scratch hardness and friction of a soft rigid–plastic solid. Tribology International 1993;26:183–93.
[9] Bressan JD, Tramontin A, Rosa C. Modeling of nanoindentation of bulk and thin film by finite element method. Wear 2005;258:115–22.
[10] Wei PJ, Tsai PW, Lin JF. Micro-contact analysis for the initial contact in nanoindentation tests. Tribology International 2008;41:1247–54.
[11] Kalidindi SR, Pathak S. Determination of the effective zero-point and the extraction of spherical nanoindentation stress–strain curves. Acta Materialia 2008;56:3523–32.
[12] Grau P, Berg G, Fränzel W, Meinhard H. Recording hardness testing. Problems of measurement at small indentation depths. Physics Status Solidi A 1994;146:537–48.
[13] Ullner C. Requirement of a robust method for the precise determination of the contact point in the depth sensing hardness test. Measurement 2000;27:43–51.
[14] Hochstetter G, Jimenez A, Cano JP, Felder E. An attempt to determine the true stress–strain curves of amorphous polymers by nanoindentation. Tribology International 2003;36:973–85.
[15] Mourhatch R, Aswath PB. Tribological behavior and nature of tribofilms generated from fluorinated ZDDP in comparison to ZDDP under extreme pressure conditions—Part II: morphology and nanoscale properties of tribofilms. Tribology International 2011;44:201–10.
[16] Fischer-Cripps AC. Critical review of analysis and interpretation of nanoindentation test data. Surface and Coatings Technology 2006;200:4153–65.
[17] Bernhardt E.O., On microhardness of solids at the limit of Kick′s similarity law. Zeitschrift Fur Metallkunde 1941; 33: 135-144.
[18] Jost N, Schmidt I. Friction-induced martensitic transformation in austenitic manganese steels. Wear 1986;111:377–89.
[19] Oliver WC, Pharr GM. An improved technique for determining hardness and elastic modulus using load and displacement sensing indentation experiments. Journal of Materials Research 1992;7:1564–83.
[20] Bigerelle M, Mazeran PE, Rachik M. The first indenter-sample contact and the indentation size effect in nano-hardness measurement. Materials Science and Engineering C 2007;27:1448–51.
[21] Kick F., Das Gesetz der proportionalen Widerstände und seine Anwendungen: Nebst Versuchen über das Verhalten verschiedener Materialien bei gleichen Formänderungen sowohl unter der Presse als dem Schlagwerk/. Verlag von Arthur Felix,.
[22] Zeng K, Chiu C–. An analysis of load–penetration curves from instrumented indentation. Acta Materialia 2001;49:3539–51.
[23] Iost A, Bigot R. Indentation size effect: reality or artefact? Journal of Materials Science 1996;31:3573–7.
[24] Marquardt D. An algorithm for least-squares estimation of nonlinear parameters. SIAM Journal on Applied Mathematics 1963;11:431–41.
[25] Levenberg K. A method for the solution of certain non-linear problems in least squares. Quarterly Journal of Applied Mathematics 1944;2:164–8.
[26] Oliver WC, Pharr GM. Review: measurement of hardness and elastic modulus by instrumented indentation: advances in understanding and refinements to methodology. Journal of Materials Research 2004;19:3–20.
[27] Alcalá J, Barone AC, Anglada M. The influence of plastic hardening on surface deformation modes around Vickers and spherical indents. Acta Materialia 2000;48:3451–64.
[28] Haušild P, Nohava J, Pilvin P, Characterisation of strain-induced martensite in a metastable austenitic stainless steel by nanoindentation. Strain 47 (52), 129–133.
[29] Jeng Y-R, Tan C-M. Theoretical study of dislocation emission around a nanoindentation using a static atomistic model. Physical Review B 2004;69:104109.
[30] Jeng Y-R, Tan C-M. Static atomistic simulations of nanoindentation and determination of nanohardness. Journal of Applied Mechanics 2005;72:738.
[31] Bucaille JL, Stauss S, Felder E, Michler J. Determination of plastic properties of metals by instrumented indentation using different sharp indenters. Acta Materialia 2003;51:1663–78.
[32] Giannakopoulos AE, Suresh S. Determination of elastoplastic properties by instrumented sharp indentation. Scripta Materialia 1999;40:1191–8.
[33] Pulecio SAR, Farias MCM, Souza RM. Finite element and dimensional analysis algorithm for the prediction of mechanical properties of bulk materials and thin films. Surface and Coatings Technology 2010;205:1386–92.